J. Fluid Mech. (1980), *vol.* 101, *part* 3, *pp.* 583–607
Printed in Great Britain

The early stage of development of the wake behind an impulsively started cylinder for $40 < Re < 10^4$

By ROGER BOUARD AND MADELEINE COUTANCEAU
Laboratoire de Mécanique des Fluides, Université de Poitiers, France

(Received 3 January 1980)

The time development of the symmetrical standing zone of recirculation, which is formed in the early stage of the flow due to a circular cylinder impulsively set in motion perpendicular to its generators, has been studied using a flow visualization technique. The Reynolds numbers (based upon the diameter) range from 40 to 10^4. Some new phenomena indicated in the flow patterns are revealed, and several different regimes are differentiated by a detailed analysis of the evolution of the main flow characteristics. A correlation with some theoretical results is established.

1. Introduction

The time development of the flow induced by an impulsively started circular cylinder is a classic problem in fluid mechanics. But, although the geometry is simple, the phenomena appear to be complex especially for large Reynolds numbers, and the numerical solution of the corresponding motion equations is very difficult to obtain. This explains why many research workers tried a theoretical approach to this problem (see the list quoted by Coutanceau & Bouard 1977*a*,*b*) but only a few of them (Thoman & Szewczyk 1969; Son & Hanratty 1969; Collins & Dennis 1973*a*; Bar-Lev & Yang 1975; Panikker & Lavan 1975; Deffenbaugh & Marshall 1976; Patel 1976; Daube & Ta Phuoc Loc 1979; Ta Phuoc Loc 1980), treat it for finite Reynolds numbers larger than 200.

Detailed experimental results seem necessary to provide verification and guidance in developing and improving the calculation techniques. However, these experimental data are very scarce at the moment, most recent being those of Honji & Taneda (1969), Taneda (1972, 1977). These authors have given some important information about the problem, but they did not consider Reynolds numbers greater than 1800.

Using a visualization technique which we have perfected particularly in the analysis of the photographs, our object was to determine the hydrodynamic field and the main geometrical features of the recirculating zone that occurs behind a circular cylinder (of diameter D) moving with the constant speed V_0 perpendicular to its generators following an impulsive start from rest. In our earlier work (Coutanceau & Bouard 1977*a*, *b*) concerned with Reynolds numbers ($Re = V_0 D/\nu$) ranging from 5 to 40, we showed that in both steady and unsteady flow our measurements were accurate enough to allow comparisons with theoretical results. Certain calculation methods and forecasts made by some authors have been confirmed in this way and new phenomena, related in particular to the influence of the wall proximity on the evolution of the flow, have been pointed out.

The present work is concerned with the initial unsteady flow. The investigation

0022–1120/80/4600–2540 $02.00

domain is extended up to Reynolds numbers of about 10^4, and the initial phase of the flow development $0 \leqslant t^* \leqslant 3{\cdot}5$ ($t^* = tV_0/D$) is considered in detail.

2. Experimental technique

The experimental technique has been already described by Coutanceau & Bouard (1977*a*) and consists of a flow visualization fine enough to allow us to observe the detailed flow structure and also (an important point) to determine the velocity field by means of precise analysis of the photographs. The flow is produced by causing the cylinder, whose axis is horizontal, to rise vertically along the median plane of a tank with rectangular cross section. In order to obtain the desired range of Reynolds numbers, this tank is filled with a liquid of suitable viscosity ($1\text{cSt} \leqslant \nu \leqslant 40\,\text{cSt}$); vaseline oil and several water-glycerine mixtures were used.

To minimize the wall and extremity effects (bottom and free surface effects), a large tank ($56 \times 46 \times 100$ cm) was chosen and the photographs were taken when the cylinder was about half-way up the tank. The motions of the cylinder and camera are coupled by means of a T-shaped support, and are generated by a system of pulleys and balance weights. The starting is almost instantaneous ($t^* \leqslant 0{\cdot}02$) and photographs are taken successively after regular time intervals.

To obtain a good definition of the flow pattern, we use cylinders with diameters as large as possible, consistent with the wall effects remaining negligible. We have previously shown (Coutanceau & Bouard 1977*b*) that these effects depend both upon the time and Reynolds number. Since only the early stage of the flow development is considered here, cylinders with diameters ranging from 3 to 15 cm have been selected for the domain of Re considered ($40 < Re < 10^4$).

The visualization is realized with reflecting (magnesium) or diffusing (rilsan) solid tracers adapted to the fluid nature† and fine enough (they are obtained by successive decantations in the same fluid as the one used in the experiment) for satisfying the 'fidelity conditions'. The lighting is provided by a powerful arc projector (80 V, 140 A). Many photographs have been taken in these conditions, for Re varying by steps equal to 10 (or 100, or 1000) for $Re \leqslant 100$ (or $Re > 100$, or $Re > 1000$).

3. Qualitative examination of the flow pattern

Plates 1 to 8 show some examples of the flow visualizations that we have obtained.

3.1. *Generalities*

As we mentioned before (Coutanceau & Bouard 1977*a*) the outline of the cylinder is not wholly visible on the photographs because of the masking effect produced by its end section being in the camera direction. On the other hand, dark zones appear on several photographs behind the cylinder: indeed, when the cylinder remains at rest during a long enough time, the solid tracers in suspension in the liquid settle a little and then, the cylinder acting as an 'umbrella', the fluid situated immediately behind it is devoid of these visualization tracers. The dark zones visible on the photographs

† For example the magnesium particles, which are better than the rilsan particles with regard to degree of luminosity, cannot be chosen for the water mixtures because they react chemically with water.

reveal the position of this fluid, initially without tracers, at a given time after the cylinder begins to move. This phenomenon occurs only when the experiments are carried out with the liquids of lowest viscosity, i.e. essentially for pure water.

Let us consider the flow development with the time t^* and with the Reynolds number Re. Immediately after the start of the motion, the flow is irrotational everywhere. But as the cylinder moves through the fluid, vorticity is generated at the solid surface and transported to the region of the rear stagnation point, inducing a reversal flow. So for $Re > 4{\cdot}4$ and after a period of time which is the shorter as the Reynolds number becomes greater, a separation of the flow appears giving rise to a recirculating zone that grows (in width and length) with time. The present investigation is limited to the case where the recirculating zone, in which two or more eddies develop, remains symmetrical and stably attached to the cylinder.

Note that from now on symmetry of the flow will be assumed and for simplicity only half of the wake will be described.

A simple qualitative examination of the photographs shows that the time development of the flow differs when Re is increasing; in particular, beyond certain limiting values of t^* and Re, secondary phenomena appear in the recirculating zone, near the cylinder surface.

With regard to the Reynolds number, as pointed out by Coutanceau & Bouard (1979), it is possible to distinguish three categories of flow time evolutions which correspond successively to small, moderate and high Reynolds numbers:

$$4{\cdot}4 \leqslant Re \leqslant Re_{L1}, \quad Re_{L1} \leqslant Re \leqslant Re_{L2} \quad \text{and} \quad Re \geqslant Re_{L2}.$$

The exact limiting values Re_{L1} and Re_{L2} cannot be determined by this qualitative investigation; they will be specified subsequently by means of graphical representations of the main characteristics of the flow. However, for the sake of clarification, we can say now that the values of Re_{L1} and Re_{L2} have been found to be approximatively 60 and 500.

3.2. *Time evolution at low Reynolds numbers:* $4{\cdot}4 \leqslant Re \leqslant Re_{L1}$

If the value of Re remains below a certain limiting value of Re_{L1} and $t^* \leqslant 3{\cdot}5$, the flow develops with time without visible distortion and is similar to that described previously by Coutanceau & Bouard (1977*b*). After a short lapse of time, the flow separates from the cylinder and in half of the recirculating zone, a unique eddy is formed that we call 'main eddy'; for example when $Re \geqslant 20$ this main eddy occurs as soon as $t^* \leqslant 0{\cdot}4$. The length L and the width l of the wake, as well as the separation angle θ_s and the abscissa a and ordinate b of the core of the eddy (see figure 1) increase when t^* is increasing. The corresponding curves have been given by Coutanceau & Bouard (1977*b*) for Reynolds number up to $Re = 40$.

It appears that for $Re = 50$ and 60 the flows still belong to this category of low Reynolds numbers and are always stable up to $t^* = 3{\cdot}5$. But later, at a time t_I^* which is shorter as Re is greater, the wake will become unstable; we found previously that in a flow with negligible wall effects, the instability appears when $Re > 34$ (this value has been recently experimentally confirmed by Gerrard 1978). Figure 1 of plate 1 of Coutanceau & Bouard (1977*b*) presents this sort of structure for $Re = 42{\cdot}8$ and $1{\cdot}1 \leqslant t^* \leqslant 6{\cdot}1$.

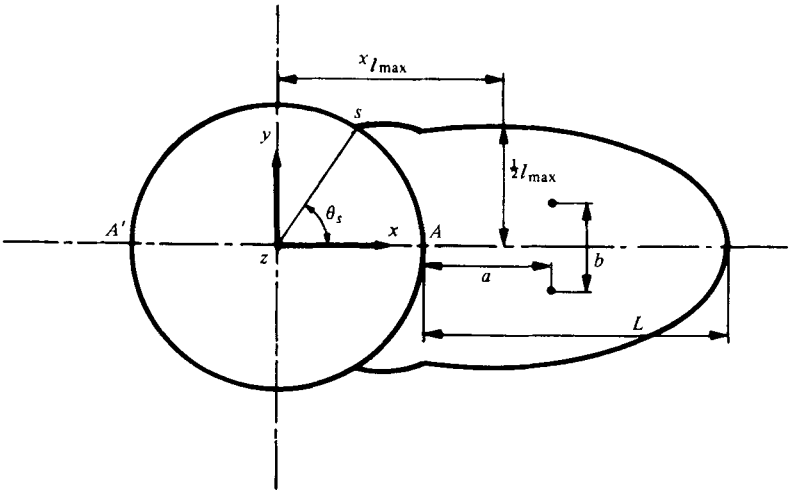

FIGURE 1. Geometrical parameters of the closed wake.

3.3. *Time evolution at moderate Reynolds numbers* $Re_{L1} \leqslant Re \leqslant Re_{L2}$

As the Reynolds number is increased the velocities in the recirculating zone increase rapidly, and then, for $Re > Re_{L1}$ secondary phenomena appear during the flow development. First, near the wall and about half-way between the stagnation and the separation points, the streamlines show some distortion: the fluid particles passing through this region deviate from the cylinder causing a bulge (figure 2*a*) in the streamline pattern and a relatively marked reduction of the velocities. This phenomenon, the amplitude of which is increased with Re, is visible for values of t^* starting from 1 and for Re ranging from 100 to 400. For greater values of Re ($500 \leqslant Re \leqslant 800$) and for $t^* \geqslant 1$, this bulge gives rise to closed streamlines forming a little secondary eddy (figure 2*b*) so that the particles are forced to follow tortuous trajectories to pass around it; the 'bulge' and the secondary eddy appear clearly for $t^* = 2{\cdot}5$ respectively in figure 3(*a*) ($Re = 300$) and 3(*b*) ($Re = 550$) of plate 1. It should be noted that in this range of Re the formation of the bulge precedes the secondary eddy and is visible for $t^* = 1$.

The secondary eddy, which has a rotation opposite to that of the main eddy, is due to a second separation of the flow, i.e. a separation from the cylinder wall of the back flow itself. (This occurs when the velocities in the recirculating zone are high enough); it grows in size when both time and Reynolds number increase.

The presence of these secondary phenomena, which do not seem to have been previously detected experimentally, indicates that the distribution of the strength ξ of the vorticity over the surface of the cylinder (which corresponds to the tangential velocity gradient) does not remain smooth as it would be for low Re. For low Re the vorticity is negative in the whole separated zone; it decreases from zero (at the rear stagnation point), reaches a minimum and regularly increases to take again a zero value at the point of separation S; beyond S, ξ is positive and still increasing up to the front stagnation point. The appearance of the bulge in the streamline pattern must give rise to an alteration in the vorticity of distribution and the 'birth' of a secondary eddy must be indicated by a positive vorticity in the separated zone. This is very well

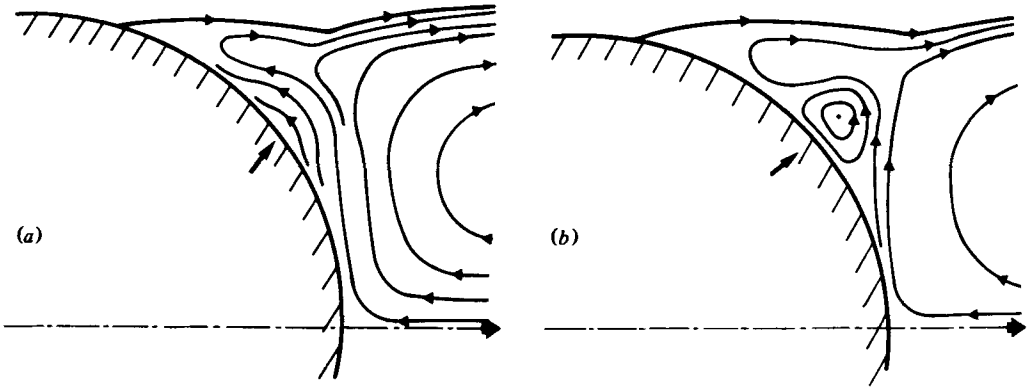

FIGURE 2. Schematic representations of the secondary phenomena: (*a*) bulge phenomenon; (*b*) isolated secondary eddy.

confirmed by numerical calculations of Son & Hanratty (1969), Collins & Dennis (1973*a*) and Patel (1976); indeed their curves of vorticity present a 'kink' for $Re = 100$ and $t^* \geqslant 2$ (*C* and *D*) or $t^* \geqslant 1{\cdot}54$ (*P*) and for $Re = 200$ and $t^* \geqslant 1{\cdot}75$ (*S* and *H*) or $t^* \geqslant 1{\cdot}27$ (*P*). On the other hand, for $Re = 500$, the three calculations first show this kink for $t^* \geqslant 1$ and then for $t^* \geqslant 1{\cdot}59$ (*C*, *D*, *S*, *H*) or $t^* \geqslant 2{\cdot}27$ (*P*) a region of positive vorticity appears in the wake so that the curve of the wall vorticity passes through two minima in this zone.

These features have also been pointed out by Patel for other Reynolds numbers ($Re = 550$ and 600) and a correlation with the corresponding streamline patterns has been established by this author for $Re = 200$, 500, 550, 600. Collins & Dennis (1973*a*) also gave streamline patterns for $Re = 500$ at different stages of the time development and localized with precision the secondary eddy.

On the other hand, it appears from our experiments that the flow in the recirculating zone is still stable at $t^* = 3{\cdot}5$ for this range of moderate Reynolds numbers.

3.4. *Time evolution at high Reynolds numbers* $Re > Re_{L2}$

Beyond the limiting value Re_{L2} two different sorts of phenomena (α and β say) occur and complicate the time development of the flow.

Phenomenon α: after a certain lapse of time following the starting of the cylinder ($t^* \geqslant 1{\cdot}5$) and when the main eddy is still stable, the secondary eddy is enough developed in size for its exterior boundary to touch the boundary of the main recirculating zone thus splitting the main eddy into two parts and isolating the region of the wake next to the separation point in which another secondary eddy is formed (figure 4*a*). These two secondary eddies thus formed are equivalent in size and in strength and constitute 'a pair of secondary eddies'. This phenomenon α which is distinctly visible from $Re = 800$ to $Re = 5000$ has also been experimentally observed by Honji & Taneda (1969) and Taneda (1972) for $Re \leqslant 1800$ and indicated by the numerical calculation of Thoman & Szewczyk (1969) who gave a good qualitative description of the time evolution of this phenomenon but for a greater value of Re (4×10^4) than those considered here. This type of flow structure is shown in figure 5 (plate 2) for $Re = 3000$ and $t^* = 2{\cdot}5$.

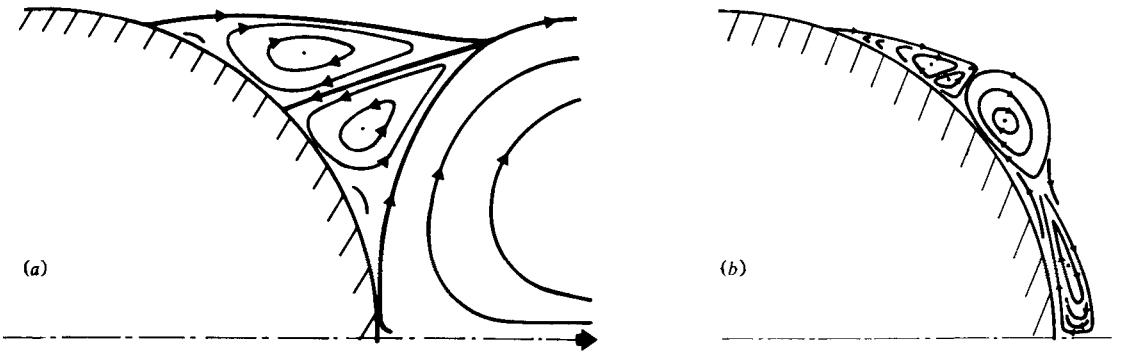

FIGURE 4. Schematic representation of the secondary eddy pair:
(*a*) phenomenon α; (*b*) phenomenon β.

Phenomenon β: at the very early phase of the flow establishment ($t^* < 1{\cdot}5$), the successive visualization photographs show a complex time development of the wake which is particularly clear for $Re = 9500$ (figures 6*a–d*, plates 3–6). First, for $t^* = 0{\cdot}5$ a very thin recirculating wake (fitting exactly the cylinder shape) is formed, but very soon ($t^* = 0{\cdot}75$) next to the cylinder wall, the core of this recirculating zone (which seems to correspond to a vorticity peak) rotates in one piece, very quickly in comparison with the velocities in the other part of the separated zone, and is individualized in a 'vortex' that is increasing with time in size and strength. Then at $t^* = 1$, this particular vortex separates the initial wake into two parts. The one situated near the separated point S is occupied by a pair of secondary eddies whose structure is roughly similar to those described before but which however differ in details (figure 4*b*). The second part remains more or less in communication with the rapid rotating vortex. For $t^* = 1{\cdot}25$ it is seen that the vortex progressively replaces the initial wake 'absorbing' the zones on either side, including the one occupied by the pair of secondary eddies. At $t^* = 1{\cdot}5$, the initial wake, which we propose to call the 'forewake', has practically vanished and the 'main wake' is formed. Immediately after, the flow becomes unstable so that the separation of the back flow described (phenomenon α) does not occur at this value of Re of 9500. But for $Re = 5000$ these two phenomena (α and β) can be successively observed (figures 7*a–d*, plates 7 and 8); so at $t^* = 1$ a first pair of secondary eddies appears, then disappears when t^* is increasing because of the destruction of the forewake (for example, this pair of eddies is completely destroyed for $t^* > 1{\cdot}5$ and a new wake – the main wake – is formed). When t^* is still increasing another pair of secondary eddies appears (visible for $t^* = 2$ and $2{\cdot}5$) when the velocities in this main wake are high enough to cause a separation of the back flow. Afterwards ($t^* \geqslant 2{\cdot}5$) this second pair of eddies is destroyed in its turn because of the instability of the flow.

This particular flow evolution in the very early phase of the flow development when $Re \geqslant 5000$ can be compared with the one visualized on the free surface of a liquid by Prandtl & Tietjens (1934) for a moving bluff body. We found that it exists also when $Re < 5000$, but since the vortex is nearer the stagnation point as Re is lower, the

evolution is very rapid and the corresponding phenomenon is then less distinctly observable. Thus for Re ranging from 1000 to 3000, the existence of the first pair of secondary eddies has not been clearly shown by visualization though the development of the forewake is already visible. On the other hand for this range of Re the second pair of secondary eddies appears to be very well formed for t^* ranging from 1·5 to 3.

It is important to note that in all cases the formation of the secondary eddy pair is due to a division of the recirculating zone but the cause of this division is different according to whether it corresponds to the very early phase of the motion ($t^* \leqslant 1$) or to the later phase ($t^* \geqslant 1{\cdot}5$). On the other hand it appears that the formation of the forewake appreciably delays the flow development in its first phase.

Finally, the sedimentation of the visualization tracers (§ 3.1) shows clearly that the fluid composing the two secondary eddies of the two pairs (phenomena α and β) does not have the same origin: in all cases, one of the eddies is devoid of tracers in contrast with the other.

4. Evolution of the main flow characteristics in the recirculating zone

4.1. *Evolution of the exterior boundary*

In order to give an overview of the phenomenon, we show (figures 8–10) the time evolution of the shape of exterior boundary of the 'recirculating zone' or 'closed wake' for different values of the Reynolds number, which are selected to illustrate the various types of flow.

From figure 8, it is seen that for $Re = 60$ the outlines of the closed wake are classic ones, they start from the cylinder without presenting any variation in their concavities and remain smooth until their downstream extremities. It can also be seen that in the earlier stage of the flow development the point of separation moves very quickly upstream but from $t^* = 2$ the evolution becomes very slow. Concerning the maximum width of the wake, at this value of Re it remains smaller than or at most (for $t^* = 3$) equal to the cylinder diameter.

For $Re = 200$ two remarkable phenomena must be mentioned. At a fixed time t^*, the length of the recirculating zone is always shorter than the corresponding length at $Re = 60$,† the absolute value of the difference increasing as t^* is greater. On the other hand for $t^* > 1{\cdot}5$, the boundary of the closed wake shows a slight kink near the separation point dividing this boundary into two parts. In the first part the width of the wake remains smaller than the cylinder diameter D whereas it becomes slightly larger than D in the second part. The presence of the kink can be compared with the bulge phenomenon noticed in figure 3(*a*) (plate 1).

In figure 9 the outlines of the wake have been drawn for $Re = 550$ and $Re = 3000$: the length of the wake continues to decrease when Re is increasing, so this length is shorter for $Re = 3000$ than for $Re = 550$ which is itself notably shorter than the length obtained for $Re = 200$. Notice also that the kink of the exterior boundary becomes more marked as Re increases; it first appears at $t^* = 1{\cdot}5$ when $Re = 550$ and at $t^* = 1$ when $Re = 3000$ and it slightly moves downstream when t^* increases.

† The fact that the recirculating wake can, at a fixed time, be shorter when the Reynolds number is greater was produced from the calculations of Thoman (1966); his figure 44 clearly indicates this phenomenon for $Re = 4 \times 10^4$, compared with $Re = 200$.

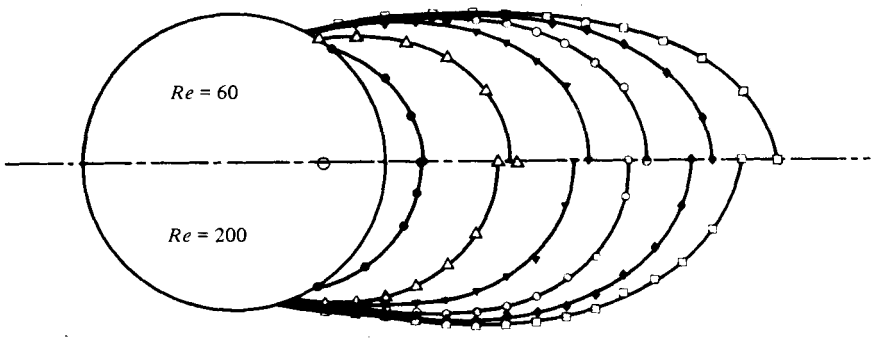

FIGURE 8. Evolution with time of the shape of the closed wake boundary for $Re = 60$ and $Re = 200$: ●, $t^* = 0{\cdot}5$; △, $t^* = 1$; ▲, $t^* = 1{\cdot}5$; ○, $t^* = 2$; ◆, $t^* = 2{\cdot}5$; □, $t^* = 3$.

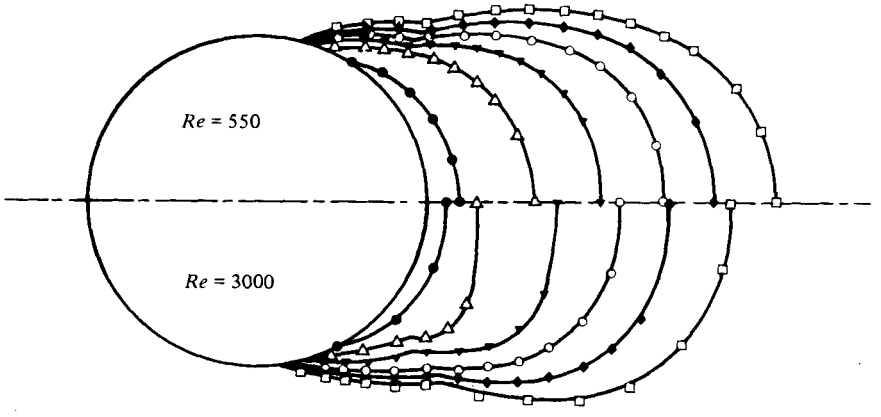

FIGURE 9. As for figure 8; $Re = 550$ and $Re = 3000$.

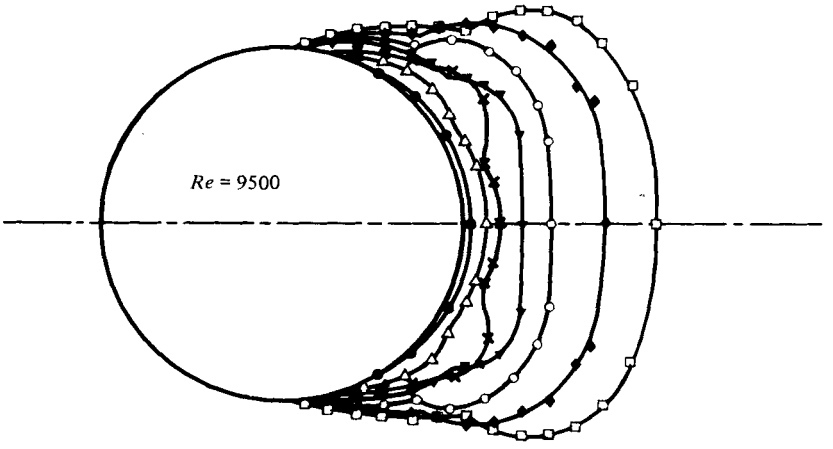

FIGURE 10. Evolution with time of the shape of the closed wake boundary for $Re = 9500$: ●, $t^* = 0{\cdot}5$; △, $t^* = 0{\cdot}75$; ×, $t^* = 1$, ▼, $t^* = 1{\cdot}25$; ○, $t^* = 1{\cdot}50$; ◆, $t^* = 1{\cdot}75$; □, $t^* = 2$.

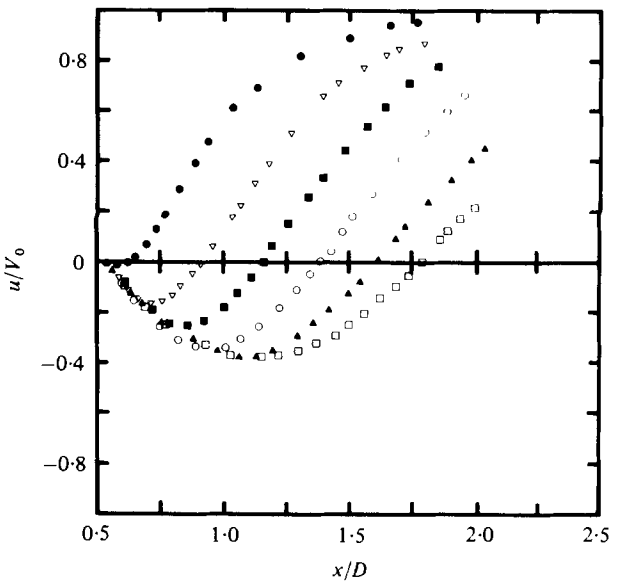

FIGURE 11. Velocity distribution on the flow axis for $Re = 60$: ●, $t^* = 0{\cdot}5$; ▽, $t^* = 1$; ■, $t^* = 1{\cdot}5$; ○, $t^* = 2$; ▲, $t^* = 2{\cdot}5$; □, $t^* = 3$.

In these two cases, the width of the wake becomes clearly larger than the cylinder when $t^* > 1{\cdot}5$ and for the last value of the time considered ($t^* = 3$) the second part of the wake is larger than the first part. On the other hand for $Re = 3000$ and $t^* = 1$, the downstream extremity of the wake is flattened. If we refer to the corresponding photographs we see that this particular shape is due to the formation of the 'rapid vortex' which is giving rise to the main wake.

Figure 10 presents the case $Re = 9500$. Here the time intervals are smaller, i.e. $\Delta t^* = 0{\cdot}25$ instead of $0{\cdot}50$. It appears immediately that in the first stage ($t^* = 0{\cdot}5$) the wake is very thin and fits well the shape of the cylinder, whereas during the period $1{\cdot}25 \leqslant t^* \leqslant 2$ the second part of the wake is very flat. It is at $t^* = 1{\cdot}25$ that this fact is most obvious. For smaller time values $0{\cdot}5 < t^* < 1{\cdot}25$ the boundary of the wake is irregular and presents undulations which result from the complex structure of the flow in this recirculating zone (§3.4).

4.2. *Evolution of other characteristics*

Having made a comprehensive study by examining the shape of the wake boundary, we now consider the detailed structure of the flow by successively analysing its other significant characteristics, viz. the velocity distribution on the wake axis, the time evolution of the magnitude and localization of the maximum velocity on this axis, the length and width of the wake; and the localization of the core of the main eddy.

(*a*) *Detailed structure for* $Re = 60$. Using the technique described by Coutanceau & Bouard (1977*a*) we have accurately obtained the velocities on the flow axis. The corresponding curves are shown for $Re = 60$ in figure 11. Note that the part of the curves below the x axis corresponds to the returning flow in the wake. The length of the recirculating zone is then given by the abscissa of the second zero velocity point and can be measured with precision from these graphs. We see that when t^* increases,

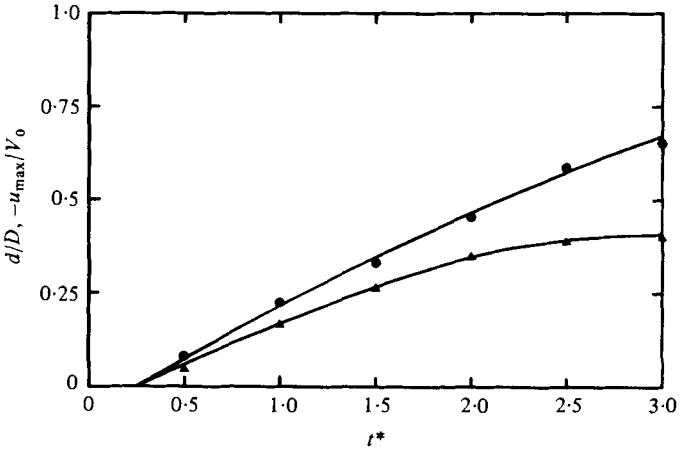

FIGURE 12. Evolution with time of the magnitude and of the location of the velocity maximum in the closed wake for $Re = 60$: ▲, $-u_{max}/V_0$; ●, d/D.

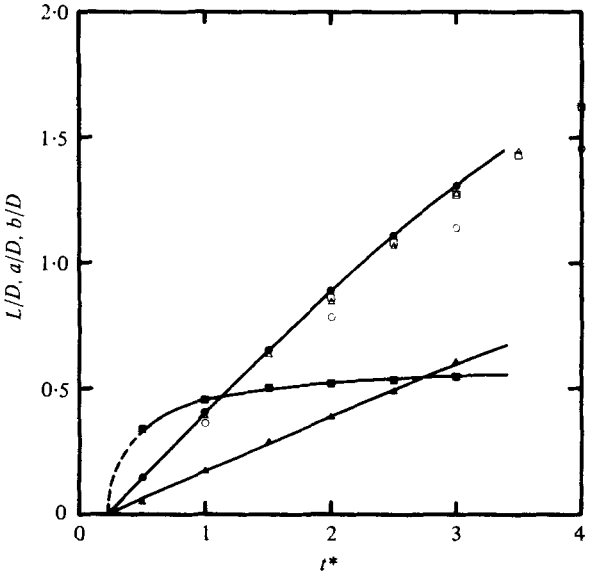

FIGURE 13. Evolution with time of the closed wake length and of the co-ordinates (a, b) of the main eddy core for $Re = 60$. Present experimental results: ●, L/D; ▲, a/D, ■, b/D. Numerical data for L/D: △, Kawaguti & Jain (1966); □, Jain & Rao (1969); ○, Patel (1976).

the velocity curves fit well together with an increase of the negative velocity maximum.

This velocity maximum constitutes an interesting parameter and therefore we have determined its value u_{max} and its localization d; the respective time evolutions of $-u_{max}$ and d are shown in figure 12. It appears that the curve of $-u_{max}$ is increasing regularly up to $t^* \simeq 2$, then is orientated towards a maximum approximately equal to $0{\cdot}4\,V_0$ for $t^* \simeq 3$. This phenomenon of the passage through a maximum for $-u_{max}$ has already been mentioned by Coutanceau & Bouard (1977*b*) for $Re \leqslant 40$. We have established that this maximum increases relatively when Re varies from 40 to 60 than for lower Re: so the increase is $\simeq 0{\cdot}12$ for $20 \leqslant Re \leqslant 40$ and $0{\cdot}23$ for $40 \leqslant Re \leqslant 60$. The

t^*		1	1·5	2	2·5	3
$Re = 60$	$x_{l\max}/D$	0·41	0·55	0·67	0·77	0·86
	$l_{\max}/D$	0·86	0·93	0·97	0·99	1·00
$Re = 200$	$x_{l\max}/D$	0·35	0·51	0·65	0·76	0·86
	$l_{\max}/D$	0·94	0·97	1·02	1·07	1·10
$Re = 550$	$x_{l\max}/D$	0·30	0·50	0·66	0·76	0·85
	$l_{\max}/D$	0·94	0·98	1·03	1·10	1·16
$Re = 3000$	$x_{l\max}/D$	0·19	0·26	0·40	0·73	0·84
	$l_{\max}/D$	0·93	0·98	1·04	1·11	1·20

TABLE 1. Numerical values of the magnitude and of the abscissa of the maximum width for various Re and t^*†.

† Since these quantities have been experimentally measured, the corresponding values are given within a certain tolerance (several per cent). On the other hand, at $t^* = 0{\cdot}5$ the closed wake width does not present a maximum and for $Re > 60$, when the wake is composed of two parts, the width is a maximum first in the first part and then in the second part.

abscissa d of the velocity maximum evolves regularly and moves away from the rear stagnation point almost linearly.

The length of the recirculating zone and the co-ordinates a and b of the core of the main eddy (see figure 1) are given in figure 13. For the length the data from theoretical investigations† have also been plotted. This length increases regularly and a good correlation exists with the data of Kawaguti & Jain (1966), Jain & Rao (1969). However, the values of Patel are lower ($\simeq 10\%$) than ours.

The abscissa a, representing the longitudinal distance between the rear stagnation point and the line of the eddy centres, changes approximately in direct proportion with t^*, whereas the tranverse distance b between the centres is rapidly increasing during the first moments of the flow establishment and then evolves very slowly from $t^* = 2$. The evolution of the width of the recirculating zone is similar. This is effectively shown in table 1 where the values of the maximum width $l_{\max}$ and the abscissa of this maximum $x_{l\max}$ are given. The behaviour of these two last parameters is comparable to those obtained for $Re = 40$, but at $t^* = 3$, $l_{\max}$ becomes almost equal to the cylinder diameter, the wake being still symmetrical. For larger values of t^*, as pointed out in previous work (Coutanceau & Bouard 1977*a*), the width tends to become larger than the cylinder but then the wake turns asymmetrical.

It can also be noticed that the time t_s^* corresponding to the origins of the representative curves of L and a ($L = a = 0$) is the same; t_s is the time at which the flow begins to separate from the cylinder and then corresponds to the 'birth' of the closed wake. On the other hand, the abscissa of the right section where the width of the wake is a maximum moves regularly downstream when t^* is increasing; for $t^* = 3$, it is situated approximately at $0{\cdot}36\,D$ from the rear stagnation point and thus at $0{\cdot}28\,L$.

(*b*) *Detailed flow structure for* $Re = 200$. The evolutions of the same flow characteristics as those described before are presented from figures 14–16 for $Re = 200$. It appears that in the recirculating zone, the velocities increase with time more rapidly than when $Re = 60$, especially for $t^* < 2$ and that the velocity maximum $-u_{\max}$ takes values which are, for $t^* = 3$, of the same order as the free stream velocity V_0: so for

† The values read from the curves of the cited authors may not be accurate because in some cases they have been printed on a small scale.

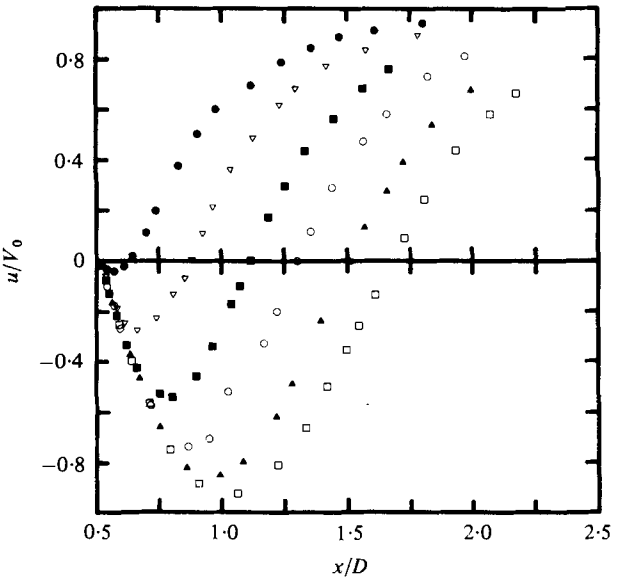

FIGURE 14. As for figure 11; $Re = 200$.

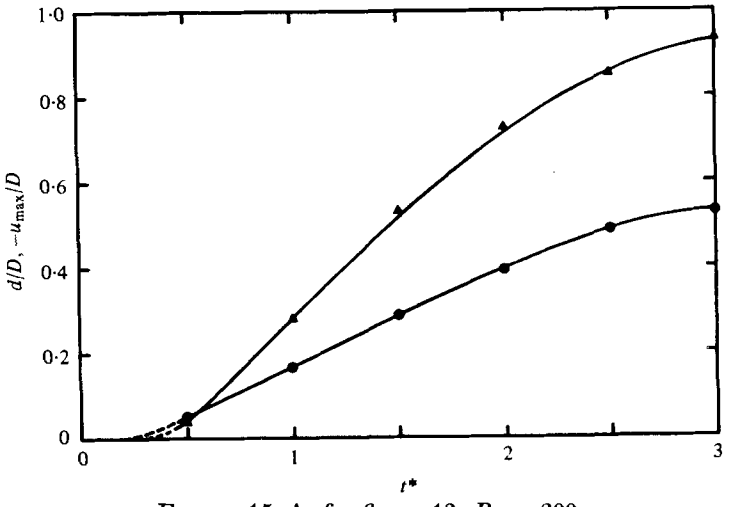

FIGURE 15. As for figure 12; $Re = 200$.

$Re = 200$, the maximum of $-u_{max}$ amounts to $0{\cdot}93\,V_0$. As a consequence of the development of these large velocities in the wake secondary effects appear such as the bulge phenomenon mentioned in §3.3. This bulge is visible for $t^* > 2$ and its localization remains almost fixed at $\theta_B \simeq 43°$.

The length of the closed wake is compared in figure 16 with the theoretical data of Jain & Rao (1969), Son & Hanratty (1969), Collins & Dennis (1973*a*), and with the experimental data of Honji & Taneda (1969) and Taneda (1972). The latter completely coincide with our data; those of Collins & Dennis and Jain & Rao also agree

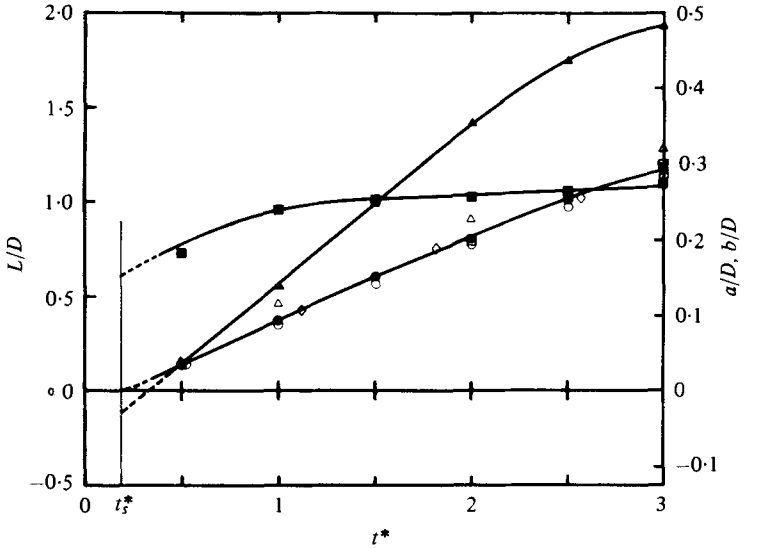

FIGURE 16. Evolution with time of the closed wake length and of the co-ordinates (a, b) of the main eddy core for $Re = 200$. Present experimental results: ●, L/D; ▲, a/D; ■, b/D. Other experimental data for L/D: ◇, Honji & Taneda (1969) and Taneda (1972). Numerical data for L/D: □, Jain & Rao (1969); △, Son & Hanratty (1969); ○, Collins & Dennis (1973*a*).

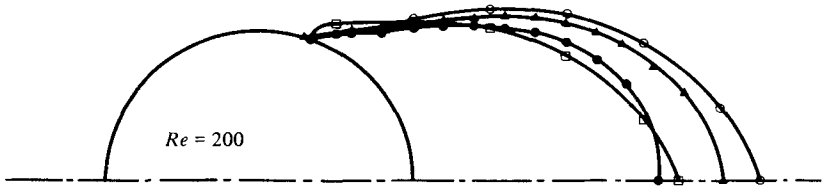

FIGURE 17. The shape of the closed wake boundary at $Re = 200$. Present experimental results: ●, $t^* = 2$; ▲, $t^* = 2{\cdot}5$. Numerical data: □, $t^* = 2{\cdot}02$, Patel (1976); ○, $t^* = 2{\cdot}65$, Son & Hanratty (1969).

well. The points given by Son & Hanratty fall above our curve. An analogous comparison is also indicated in figure 17 for the exterior wake boundary.

In figure 16 a new phenomenon is shown: the curves of the wake length L and of the main eddy core abscissa a do not intersect on the t^* axis. This fact, which will appear still more clearly for greater Re, indicates the formation of the forewake described in §3. The vertical line drawn in figure 16 corresponds to the value t_s^* of the initial separation deduced from figure 32 presented later in §5.

The parameters $l_{\max}$ and $x_{l\max}$ are given in table 1. The width of the wake becomes larger than the cylinder for $t^* > 1{\cdot}5$ (e.g. at $t^* = 3$ $l_{\max}$ is approximately equal to $1{\cdot}1\,D$); note that the phenomenon of the bulge of the streamline pattern appears precisely at $t^* = 1{\cdot}5$. For the different studied values of t^* the abscissa $x_{l\max}$ are almost the same as those given for $Re = 60$; so at $t^* = 3$ the maximum width is situated at a distance of the rear stagnation point which is still approximatively $0{\cdot}36\,D$, corresponding in this case to $0{\cdot}32\,L$.

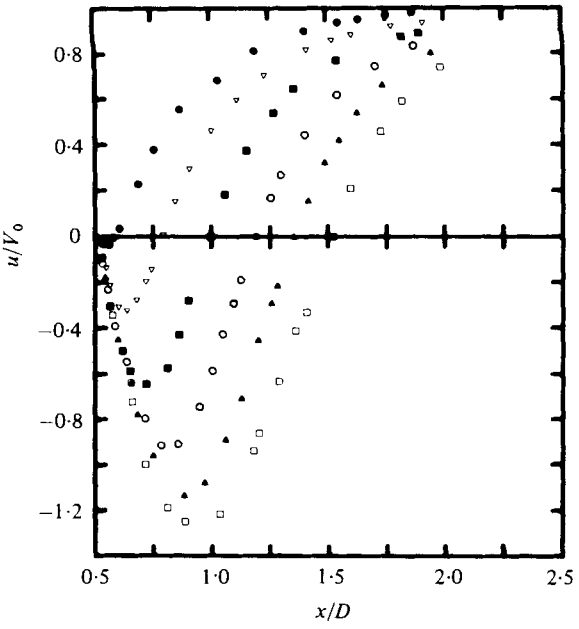

FIGURE 18. As for figure 11; Re = 550.

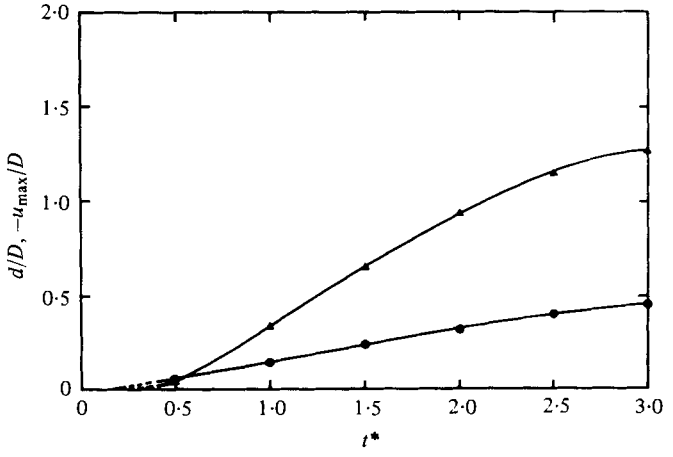

FIGURE 19. As for figure 12; Re = 550.

(c) *Detailed structure for* Re = 550. For Re = 550, the detailed structure of the flow is given in figures 18–21. This is an interesting case because it has been studied by several authors and, as shown in § 3, it corresponds to the appearance of a secondary eddy on the upstream side of the main eddy.

Figures 18 and 19 give respectively the velocity repartition on the flow axis and the time evolution of $-u_{max}$. It can be observed from these figures that for $t^* > 2$ the velocities in the wake may become larger than V_0: e.g. for $t^* = 3$, $-u_{max} \simeq 1{\cdot}26\,V_0$.

The time evolution of the length L is compared (figure 20) with data given in the literature. Among the experimental studies, those of Honji & Taneda (1969) and

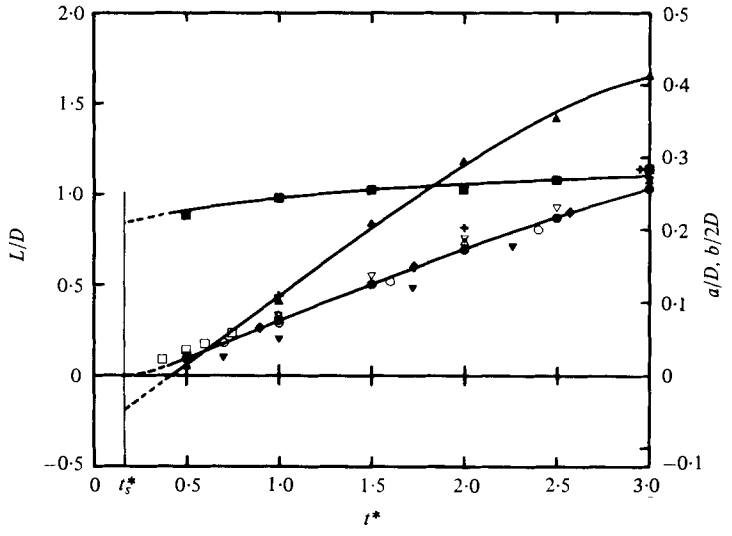

FIGURE 20. Evolution with time of the closed wake length and of the co-ordinates (a, b) of the main eddy core for $Re = 550$. Present experimental results: ●, L/D; ▲, a/D; ■, $b/2D$. Other experimental data for L/D: ▼, $Re = 560$, Schwabe (1935); ◆, $Re = 550$, Honji & Taneda (1969) and Taneda (1972). Numberical results for L/D: ▽, $Re = 600$, Thoman & Szewczyk (1969); △, $Re = 500$, Son & Hanratty (1969); ○, $Re = 500$, Collins & Dennis (1973*a*); □, $Re = 500$, Panikker & Lavan (1975); +, $Re = 500$–550–600, Patel (1976).

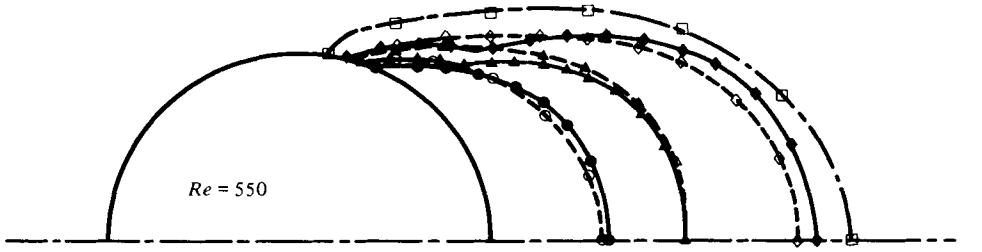

FIGURE 21. The shape of the closed wake boundary at $Re = 550$. Present experimental results: ●, $t^* = 1$; ▲, $t^* = 1{\cdot}5$; ◆, $t^* = 2{\cdot}5$. Numerical data: ○, $t^* = 1$, △, $t^* = 1{\cdot}6$; ◇, $t^* = 2{\cdot}2$ ($Re = 500$), Collins & Dennis (1973*a*); □, $t^* = 2{\cdot}54$ ($Re = 550$), Patel (1976).

Taneda (1972) agree perfectly with ours, but the earlier results of Schwabe (1935) are lower though evolving in the same way. There is satisfactory agreement with the theoretical results, except those of Patel (1976) which are notably larger.

On the other hand, as in the case $Re = 200$, it is also shown in figure 20 that the times corresponding respectively to $L = 0$ and $a = 0$ do not coincide and the difference between the two values is increasing with Re. If the curve representative of a is continued towards t_s^*, it appears that the core of the eddy must be situated upstream from the rear stagnation point A. This also agrees well with the curve giving the ordinate $\frac{1}{2}b$ of the eddy core and will be confirmed for larger values of Re.

In figure 21 a comparison is given between our experimental results for the boundary of the closed wake and theoretical data obtained by Collins & Dennis (1973) and by Patel (1976). In the case of Collins & Dennis the agreement is good, although their

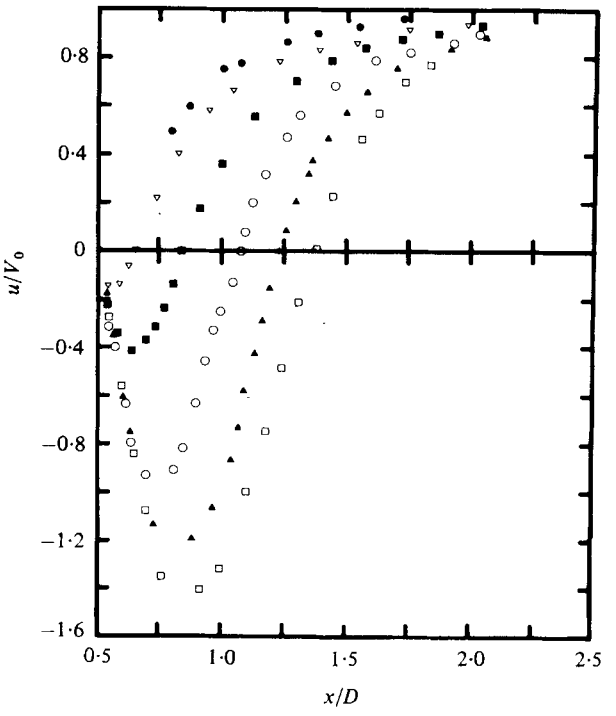

FIGURE 22. As for figure 11; Re = 3000.

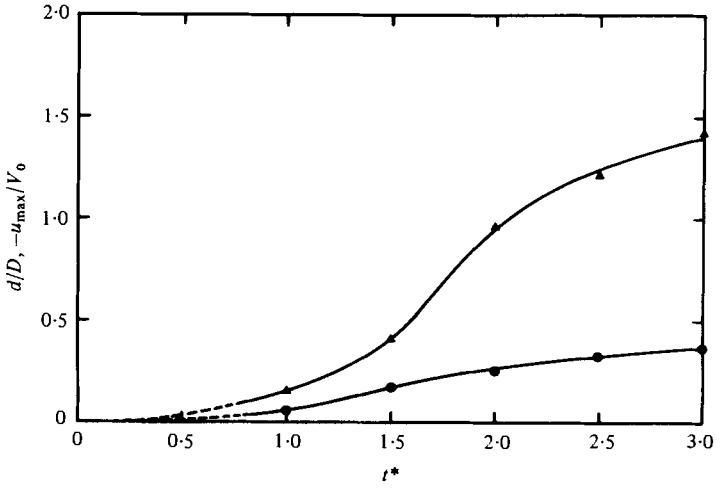

FIGURE 23. As for figure 12; Re = 3000.

results show continuous curves and the kink (seen on our visualizations for $t^* \geqslant 1{\cdot}5$) is not revealed by their calculations. The wake at $t^* = 2{\cdot}54$ given by Patel is clearly larger than the one we obtained for $t^* = 2{\cdot}5$, but the kink phenomenon is suggested and is visible in his figure 17, for $2{\cdot}54 \leqslant t^* \leqslant 28{\cdot}82$.

The presence of the kink is to be compared with the formation of the secondary eddy

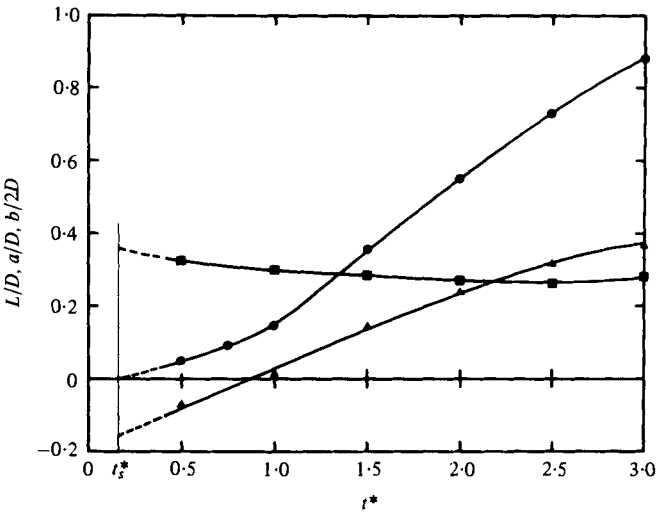

FIGURE 24. Evolution with time of the closed wake length and of the co-ordinates (a, b) of the main eddy core for Re = 3000: ●, L/D; ▲, a/D; ■, $b/2D$.

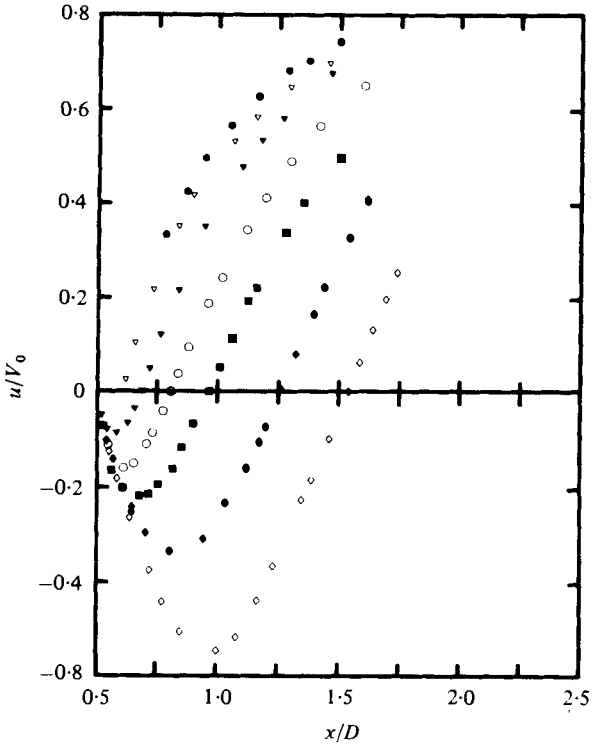

FIGURE 25. Velocity distribution on the flow axis for Re = 9500: ●, t^* = 0·5; ▽, t^* = 0·75; ▼, t^* = 1; ○, t^* = 1·25; ■, t^* = 1·5; ◆, t^* = 1·75; ◇, t^* = 2.

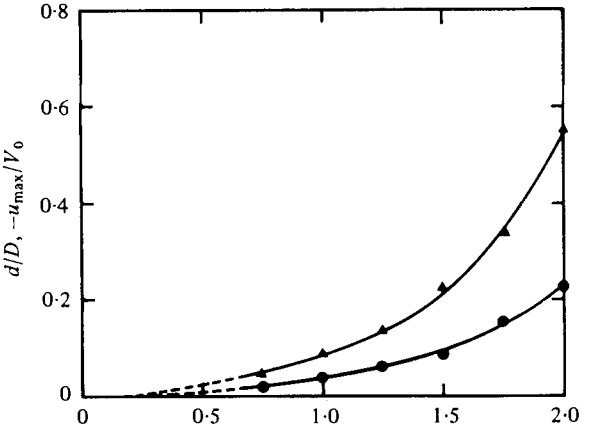

FIGURE 26. As for figure 12; Re = 9500.

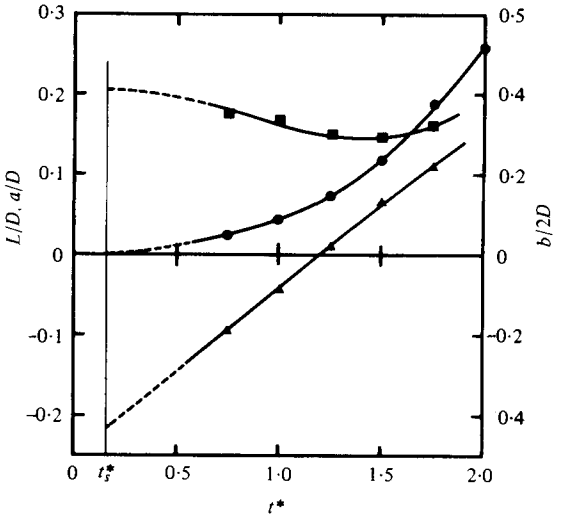

FIGURE 27. As for figure 24; Re = 9500.

whose localization is almost fixed at $\theta_E \simeq 43°$ for $1{\cdot}5 < t^* < 3$. This secondary eddy also grows in size during $1{\cdot}5 \leqslant t^* \leqslant 2$, but varies very little afterwards $2 < t^* \leqslant 3$.

Finally, for Re = 550, the maximum width measured for $t^* = 3$ is found to be approximately equal to $1{\cdot}16D$ and situated at $0{\cdot}33L$ from A.

(*d*) *Detailed flow structure for* Re = 3000 *and* 9500. Figures 22–27 present the structure of the flow for Re = 3000 and 9500. These two cases belong to the same category of flow but the phenomena are more accentuated for Re = 9500 and the destruction of the forewake occurs sooner.

We have seen above that for this range of Re, and in the first part of the studied interval of time, the wake boundary may have a typical flattened shape. The analysis of the velocity field and of the geometrical characteristics of the closed wake also shows interesting specific features.

First, let us examine the flow for Re = 3000. From figures 22 and 23 it appears that

the velocities on the flow axis increase slowly for $t^* < 1$, much more rapidly for $1 < t^* < 2{\cdot}5$, and then for $t^* > 2{\cdot}5$ the rate of increase is again reduced so that the curve of $-u_{\max}$ (figure 23) shows an inflexion at $t^* \simeq 1{\cdot}7$. At the final observation time $t^* = 3$, the magnitude of $u_{\max}$ is close to $1{\cdot}43 V_0$; thus the velocity in the wake becomes very large indeed.

The distance d (position of $u_{\max}$) increases more regularly with time, although the corresponding curve (figure 23) also shows a slight inflexion.

We recall that it is precisely for $t^* \simeq 1$ that the rapid vortex becomes visible and is already replacing the initial wake (forewake) to constitute the main wake, which is completely settled at $t^* = 2$. Resulting from the behaviour of this rapid vortex, it is seen that at $t^* = 1$ the whole recirculating fluid does not participate in the same way in the general rotation: the velocities are relatively much lower in the vicinity of the axis than near the eddy core, giving rise to high velocity gradients in this region with the core of the eddy shifting from the geometrical centre of the recirculating zone. Whereas at $t^* = 2$, when the main eddy is well formed, the core of the eddy nearly coincides with this geometrical centre and the velocities increase regularly.

This shifting of the main eddy core appears clearly on figure 24 where a significant decrease of the transverse distance b can be observed indicating that the core draws near to the flow axis as time increases. This contrasts with the cases previously considered (for lower Re values) where, in the one hand b evolves very little and on the other hand moves away from the flow axis. For $t^* \simeq 1$, figure 24 shows an abrupt change in the time evolution of the wake length L. So it is clear that this time corresponds to a change in the flow structure.

As soon as $t^* = 1{\cdot}5$, the velocities become sufficiently high in the wake for a pair of secondary eddies to develop. These eddies are localized respectively at $\theta_{E1} \simeq 43°$ and $\theta_{E2} \simeq 54°$. After an important initial growth they rapidly (from $t^* = 1{\cdot}5$) reach their maximal size and afterwards ($t^* = 3$) begin to lose their stability. Simultaneously with the occurrence of the secondary eddy pair, the width of the main wake becomes larger than the cylinder, e.g. at $t^* = 3$, $l_{\max} \simeq 1{\cdot}20 D$.

Finally, if we examine the case of $Re = 9500$, we see (from figures 25–27) that the phenomena are generally the same as in the case $Re = 3000$. However, the presence of the forewake lasts longer and the main wake becomes unstable as soon as $t^* = 2$, so that practically only the first part of the time development can be observed. In figure 27 the decrease of b is well confirmed and for $t^* < 1{\cdot}25$ significant negative values of the abscissa a (which have been measured) are plotted; for example at $t^* = 0{\cdot}75$, $a = -0{\cdot}2R$ and at $t^* = 1$, $a = -0{\cdot}09R$.

5. Recapitulatory curves and synthesis

In order to differentiate more clearly the regimes we have collected, on the same figure, the evolution of certain significant flow characteristics for various values of Re. For example, figure 28 presents, for $50 \leqslant Re \leqslant 5000$ and $t^* = 3$, the velocity distribution on the flow axis. It appears that for this fixed value of t^* and when Re is increasing, the maximum of velocity in the wake $-u_{\max}$ increases up to $Re = 2000$ and then decreases whereas the wake length passes through a maximum for $Re \simeq 60$.

Figure 29, where the variation of $-u_{\max}$ with t^* is plotted for Re ranging from 60 to 9500, confirms that, at a fixed time t^*, $-u_{\max}$ passes through a maximum. But

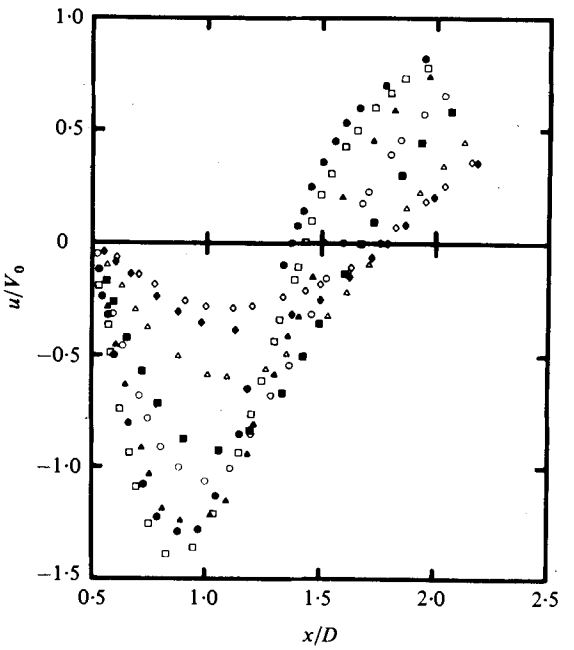

FIGURE 28. Velocity distribution on the flow axis for $t^* = 3$ and various Re: ◇, $Re = 50$; ◆, $Re = 60$; △, $Re = 100$; ■, $Re = 200$; ○, $Re = 300$; ▲, $Re = 550$; □, $Re = 2000$; ●, $Re = 5000$.

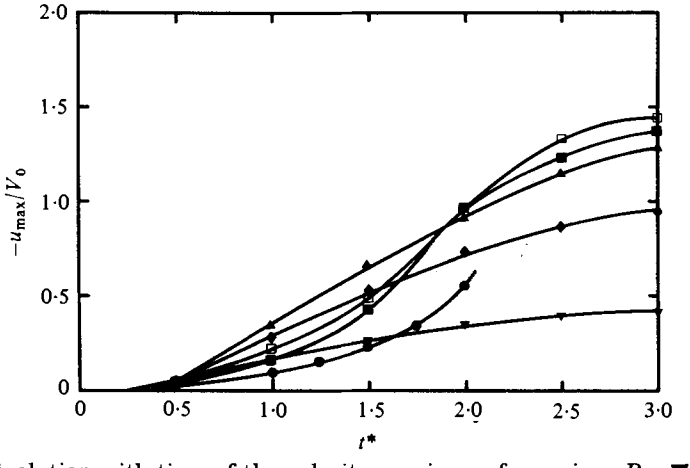

FIGURE 29. Evolution with time of the velocity maximum for various Re: ▼, $Re = 60$; ◆, $Re = 200$; ▲, $Re = 550$; □, $Re = 2000$; ■, $Re = 3000$; ●, $Re = 9500$.

because of the considerable change in the first part of the evolution when Re becomes greater than 500, the values of Re for which $-u_{max}$ reaches a maximum decreases when t^* decreases, thus, at $t^* = 3$, $-u_{max}$ is a maximum at $Re \simeq 2000$ and at $t^* = 1$, $-u_{max}$ is a maximum at $Re \simeq 500$.

The typical evolution of L is shown on figure 30 in the range $20 \leqslant Re \leqslant 9500$ where at any fixed time t^* (below the time of the initial disintegration of the wake) the wake

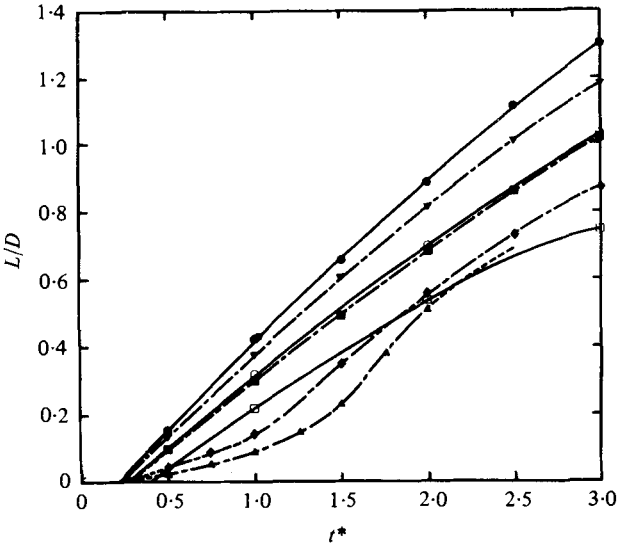

FIGURE 30. Evolution with time of the closed wake length for various Re: □, Re = 20; ○, Re = 31; ●, Re = 60; ▼, Re = 200; ■, Re = 550; ◆, Re = 3000; ▲, Re = 9500.

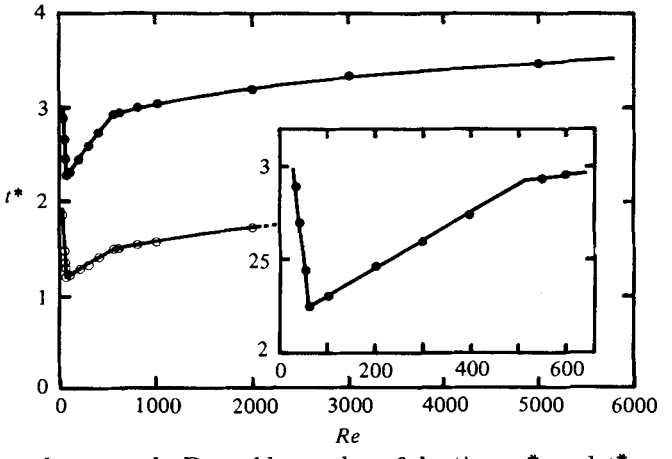

FIGURE 31. Dependence on the Reynolds number of the times $t^*_{0\cdot5}$ and t^*_1 corresponding to the formation of closed wakes whose lengths (L/D) are respectively 0·5 and 1: ○, $t^*_{0\cdot5}$; ●, t^*_1.

length is appreciably greater at Re = 60 than at any higher value of Re; e.g. at t^* = 1, 2, 3 the lengths L/D relative to Re = 60 and 3000 are 0·42 and 0·14, 0·89 and 0·55, 1·29 and 0·87 respectively.

From figure 30 it is also seen that, except in the very early phase, the time evolution of L/D is almost the same at Re = 31 and 550 and that the curve for Re = 20 intersects with both that for Re = 3000 and that for Re = 9500. So at $t^* \simeq 1\cdot8$ and 2·2 the wake length is the same for Re = 20 and 3000 and for Re = 20 and 9500, which is remarkable. On the other hand, it appears that for $Re > 550$ the time-evolution of L/D can be divided into two parts according to whether t^* is greater or less than a certain value t^*_c (for example when Re = 3000, $t^*_c \simeq 1$); the first phase corresponds to the forewake.

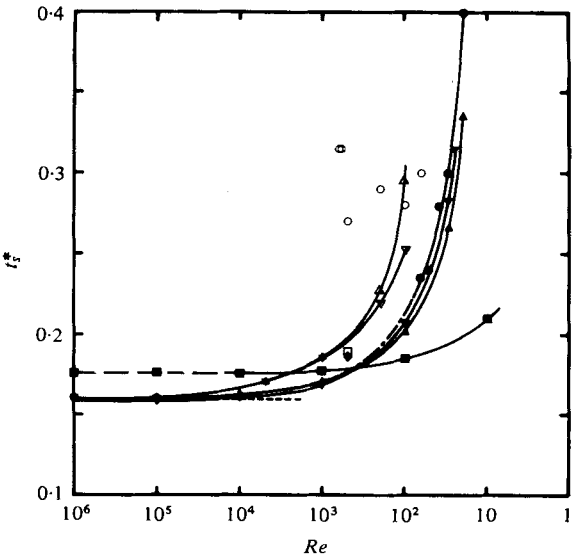

FIGURE 32. Dependence on Reynolds number of the time t_s^* corresponding to the initial separation of the flow. Present results: ●, measured values; —·—, extrapolated values. Numerical data: ——, Blasius (1908); – – –, Goldstein & Rosenhead (1936); ■, Wang (1967); □, Thoman & Szewczyk (1969); ▽, Collins & Dennis (1973*a*); △, Collins & Dennis (1973*b*); ◆, Panikker & Lavan (1975); ▲, Bar-Lev & Yang (1975); ▼, Bar-Lev & Yang (1975) – Padé approximant (2/2); ○, Patel (1976).

In figure 31, the times $t_{0.5}^*$ and t_1^* required, at a given Re, for the wake length L to reach a value equal respectively to $\frac{1}{2}D$ and to D have been plotted against Re in the range $20 \leqslant Re \leqslant 5000$ and in more detail for $20 \leqslant Re \leqslant 700$. The corresponding curves present two abrupt changes in their slopes for $Re = 60$ and $Re = 500$; it is for $Re = 60$ that the times $t_{0.5}^*$ and t_1^* are shortest. This fact, which has been verified for all values of L/D (the change in the slope being the more accentuated as L/D is greater), is in contradiction with the experimental law given by Taneda (1972). This law established that, when $t^*/Re < 0{\cdot}1$ (our results belong to this category), the time evolution of L/D would be linear and the same for all values of Re, i.e. $L/D = 0{\cdot}34t^*$; then the time necessary to obtain a fixed value of L/D should be a constant. However if we consider Taneda's points one by one, they agree very well with our curves; only his conclusion differs.

It seems that the two particular values of Re ($Re = 60$ and $Re = 500$) which correspond to the occurrence of the bulge and of the isolated secondary eddy respectively may be assigned to the limits Re_{L1} and Re_{L2} defined in § 3.1.

The variation with Re of the time t_s^* at which separation of the flow first occurs is shown in figure 32 where theoretical data have also been plotted. When $Re \leqslant 60$ the curves $L/D(t^*)$ are practically linear over their first part and we have thus been able to obtain relatively significant values of t_s^* by a simple extrapolation: these values, which decrease when Re increases, are situated between the analytical results of Bar-Lev & Yang (1975) and the numerical ones given by Collins & Dennis (1973*a*, *b*). Beyond $Re = 60$, and if the existence of the forewake was not taken into account, we would find, using the same linear extrapolation method, that t_s^* would increase instead of

decreasing towards a limit as predicted by boundary layer theory. So we thought it logical to join our experimental curve t_s^* *vs.* Re to the curves given by the theoreticians. The corresponding values of t_s^* deduced by this way agree with the prolongation of our wake length curves given in figures 16, 20, 24, 27 and even for the greatest values of Re for which the forewake existence has been effectively pointed out by the experiment.

6. Conclusion

A detailed analysis of the flow inside the recirculating zone produced by an impulsively started cylinder has identified the time evolution of the principal characteristics for $40 \leqslant Re \leqslant 10^4$, thus extending the data given in previous work by Coutanceau & Bouard (1977*b*). Some of this data has been given here for the first time, especially that for the largest values of the Reynolds number.

Three regimes have been differentiated according to whether the Reynolds number is below 60, between 60 and 500, or above 500. For $Re > 60$ some new secondary phenomena have been pointed out, viz.:

(i) the development of a bulge in the streamline pattern and of an isolated secondary eddy before (this term refers to change with respect to both time and Reynolds number) the appearance of a pair of secondary eddies;

(ii) the wake evolution in two phases, the forewake and the main wake;

(iii) the individualization of a rapid vortex during the very early phase of the evolution which gives rise to the main eddy and which occurs near the cylinder, further upstream the rear stagnation point as Re increases.

Several consequences of these secondary phenomena have also been established, for example:

(i) the presence of the bulge and of the secondary eddies causes a kink in the exterior boundary of the recirculating zone which then becomes larger than the cylinder before any asymmetry can be detected;

(ii) the appearance of the rapid vortex in the forewake produces, during the first phase of development, a flattening of the downstream part of the recirculating zone and an important reduction of its evolution, especially for the length and the velocity maximum.

Our results confirm and complete information previously given on this subject. So far as experimental work is concerned, Honji & Taneda (1969) and Taneda (1972) pointed out the formation of a pair of secondary eddies for $Re > 550$, but did not notice the existence of intermediate configurations and their important consequences particularly for the time evolution of the recirculating zone. On the other hand until recently this pair of secondary eddies, although found for $Re = 4 \times 10^4$ by Thoman & Szewczyck (1969), did not seem to be clearly established by calculations for the range of Reynolds numbers considered here†; only the flow structure, one with a bulge in the streamlines (that may be deduced from the wall vorticity curves) and the other with a unique secondary eddy, were revealed (Son & Hanratty 1969; Collins & Dennis 1973*a*; Patel 1976). It is the same for the individualization of the rapid vortex, which

† Using an efficient numerical method that they have perfected, Daube & Ta Phuoc Loc (1979) and Ta Phuoc Loc (1980) have just found the three stages of evolution (the bulge, the isolated eddy and the pair of eddies) analogous to those revealed by our experiments for similar values of Re and t^*.

has been shown by our experiments but not explicitly proved by the calculations; however we note that it coincides remarkably with the peak suddenly developed by the vorticity curves given by Thoman & Swerczyk (1969) for $Re = 4 \times 10^4$ and by Collins & Dennis (1973*a*) for $Re = 5000$. We hope that this complementary data will contribute to knowledge of this complex problem.

The authors wish to thank Prof. J.-M. Bourot, Director of the Fluid Mechanics Laboratory of Poitiers and Prof. S. C. R. Dennis of London (Canada) for their useful suggestions, J. R. Defaye for his help in translating this text into English, and P. Falaise and G. Branger for their contribution to the elaboration of efficient experimental techniques.

REFERENCES

BAR-LEV, M. & YANG, H. T. 1975 Initial flow field over an impulsively started circular cylinder. *J. Fluid Mech.* **72**, 625.

BLASIUS, H. 1908 Grenzschichten in Flüssigkeiten mit kleiner Reibung. *Z. Math. Phys.* **56**, 1. (English translation, NACA TM 1256.)

COLLINS, W. M. & DENNIS, S. C. R. 1973*a* Flow past an impulsively started circular cylinder. *J. Fluid Mech.* **60**, 105.

COLLINS, W. M. & DENNIS, S. C. R. 1973*b* The initial flow past an impulsively started circular cylinder. *Quart. J. Mech. Appl. Math.* **26**, 53.

COUTANCEAU, M. & BOUARD, R. 1977*a* Experimental determination of the main features of the viscous flow in the wake of a circular cylinder in uniform translation. Part 1. Steady flow. *J. Fluid Mech.* **79**, 231.

COUTANCEAU, M. & BOUARD, R. 1977*b* Experimental determination of the main features of the viscous flow in the wake of a circular cylinder in uniform translation. Part 2. Unsteady flow. *J. Fluid Mech.* **79**, 257.

COUTANCEAU, M. & BOUARD, R. 1979 Sur la formation de tourbillons 'secondaires' dans le sillage d'un cylindre soumis à un départ impulsif. *C. r. hebd. Séanc. Acad. Sci.* **288**, Série B-45.

DAUBE, O. & TA PHUOC LOC 1979 Méthode numérique compacte pour la simulation d'écoulements visqueux décollés stationnaires ou non. Application aux corps profilés – 16ème *Colloque d'Aérodynamique Appliquée de Lille.*

DEFFENBAUGH, F. D. & MARSHALL, F. J. 1976 Time development of the flow about an impulsively started cylinder. *A.I.A.A. Journal* **14**, 908.

GERRARD, J. H. 1978 The wakes of cylindrical bluff bodies at low Reynolds number. *Phil. Trans. R. Soc.* **288**, 351.

GOLDSTEIN, S. & ROSENHEAD, O. C. 1936 Boundary layer growth. *Proc. Phil. Soc.* **32**, 392.

HONJI, H. & TANEDA, S. 1969 Unsteady flow past a circular cylinder. *J. Phys. Soc. Japan* **27**, 1668.

JAIN, P. C. & RAO, K. S. 1969 Numerical solution of unsteady viscous incompressible fluid flow past a circular cylinder. *Phys. Fluids Suppl.* **12** (II), 57.

KAWAGUTI, M. & JAIN, P. C. 1966 Numerical study of a viscous fluid flow past a circular cylinder. *J. Phys. Soc. Japan*, **21**, 2055.

PANIKKER, P. K. G. & LAVAN, Z. 1975 Flow past impulsively started bodies using Green's functions. *J. Comp. Phys.* **18**, 46.

PATEL, V. A. 1976 Time dependent solutions of the viscous incompressible flow past a circular cylinder by the method of series truncation. *Computers and Fluids*, **4**, 13.

PRANDTL, L. & TIETJENS, O. G. 1934 *Applied Hydro and Aeromechanics*, McGraw-Hill (translated from the German edition, Springer 1931).

SCHWABE, M. 1935 Über Druckermittlung in der nichtstationären ebenen Strömung. *Ingénieur – Archiv.* **6**, 34.

SON, J. S. & HANRATTY, T. J. 1969 Numerical solution for the flow around a cylinder at Reynolds numbers of 40, 200 and 500. *J. Fluid Mech.* **35**, 369.

TANEDA, S. 1972 Visualization experiments on unsteady viscous flows around cylinders and plates. In *Récentes recherches sur les couches limites instationnaires*, vol. 2 (ed. E. A. Eichelbrenner), p. 1165. Laval University Press, Quebec.

TANEDA, S. 1977 Visual study of unsteady separated flows around bodies. *Prog. Aerospace Sci.* **17**, 287.

TA PHUOC LOC 1980 Numerical analysis of unsteady secondary vortices generated by an impulsively started circular cylinder. *J. Fluid Mech.* **100**, 111.

THOMAN, D. C. 1966 Numerical solutions of the dependent two-dimensional flow of a viscous, incompressible fluid over stationary and rotating cylinders. Ph.D. dissertation, University of Notre-Dame, Indianna.

THOMAN, D. C. & SZEWCZYK, A. A. 1969 Time-dependent viscous flow over a circular cylinder. *Phys. Fluids Suppl.* **12** (II), 76.

WANG, C. Y. 1967 The flow past a circular cylinder which is started impulsively from rest. *J. Math. Phys.* **46**, 195.

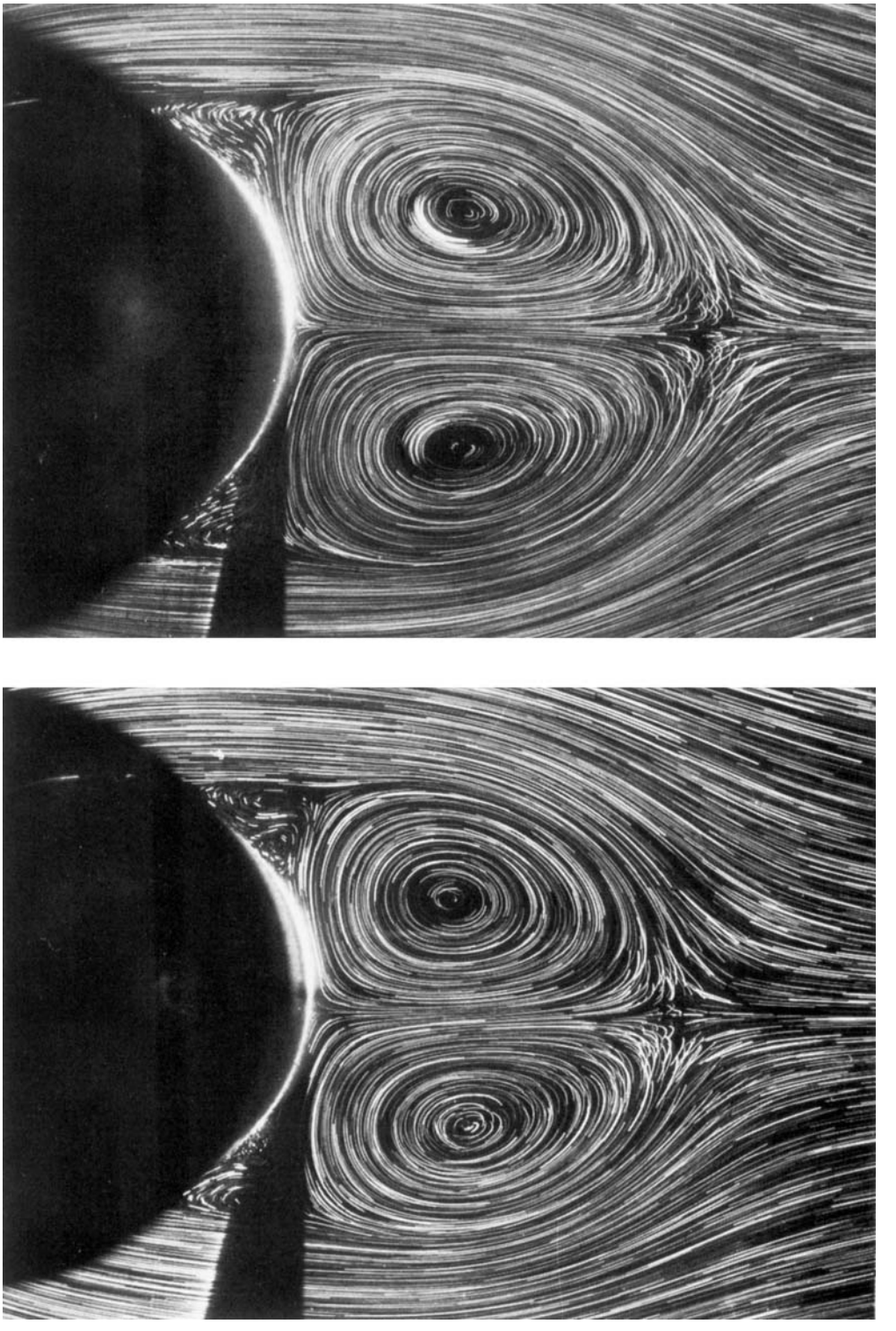

FIGURE 3. (*a*) $Re = 300$, $t^* = 2{\cdot}5$; (*b*) $Re = 550$, $t^* = 2{\cdot}5$.

FIGURE 5. $Re = 3000$, $t^* = 2{\cdot}5$.

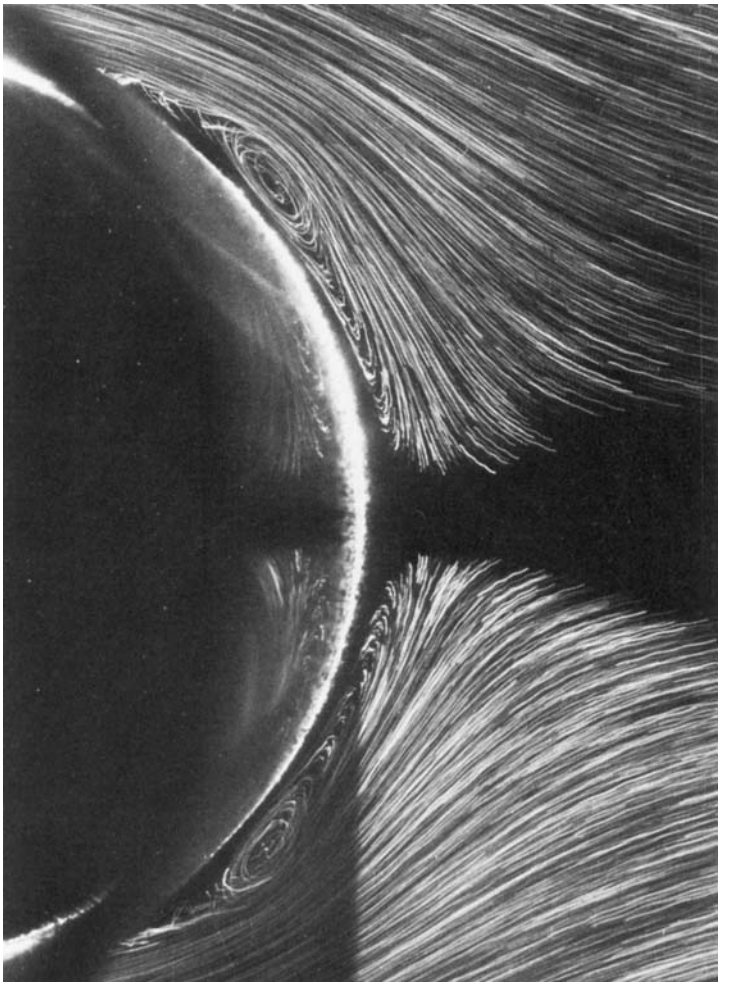

FIGURE 6 (*a*). For legend see plate 6.

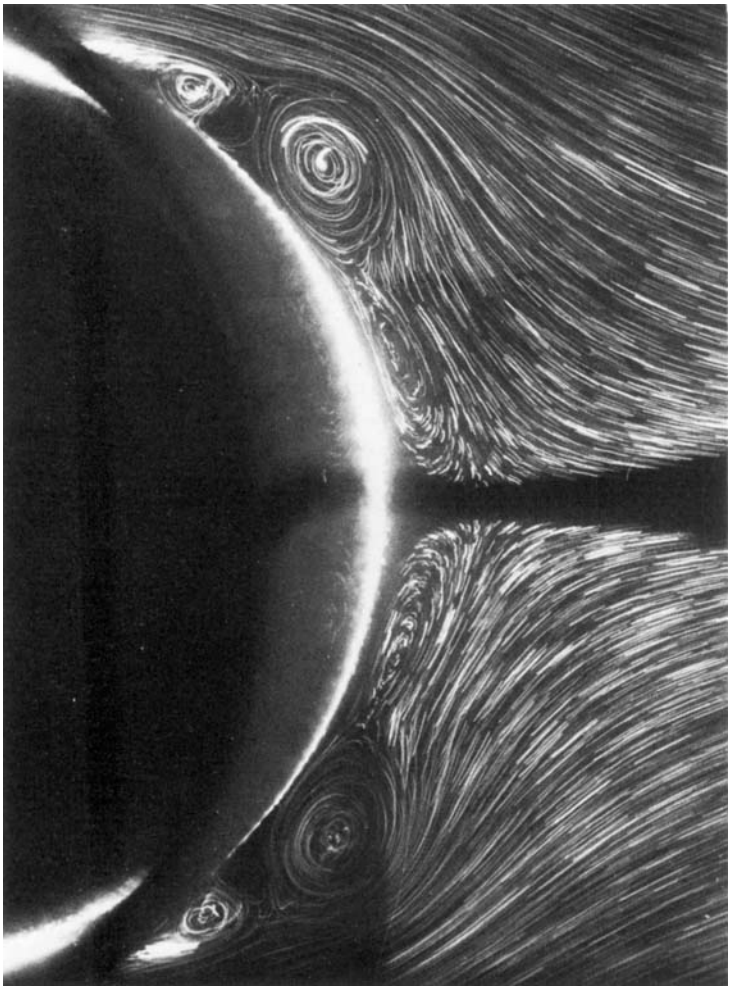

FIGURE 6 (*b*). For legend see plate 6.

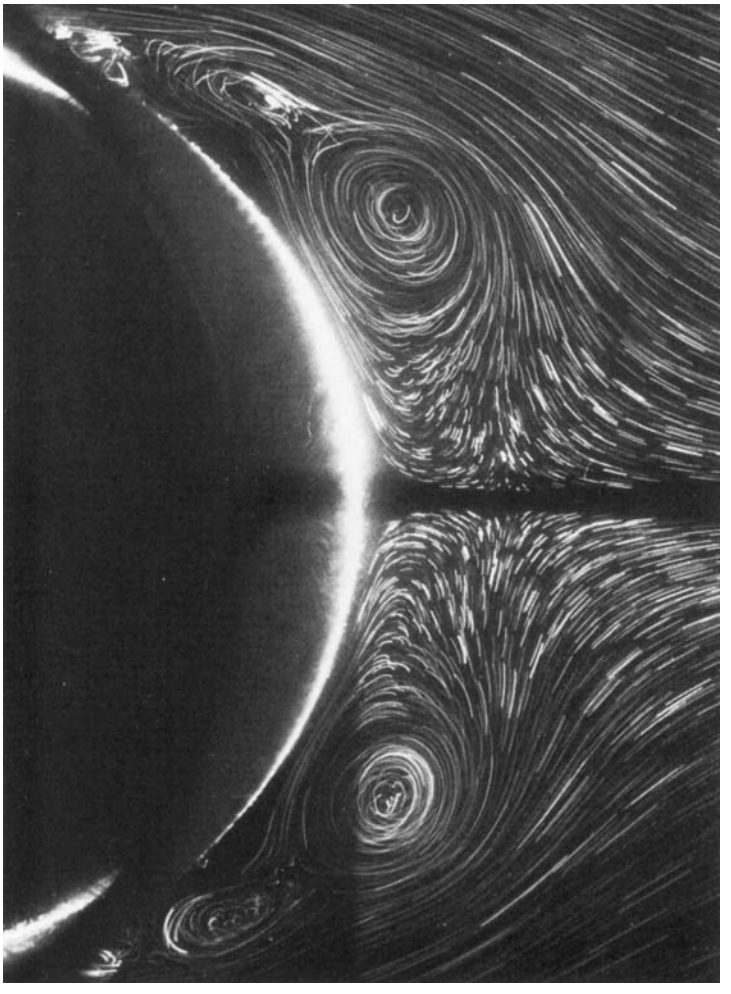

FIGURE 6 (*c*). For legend see plate 6.

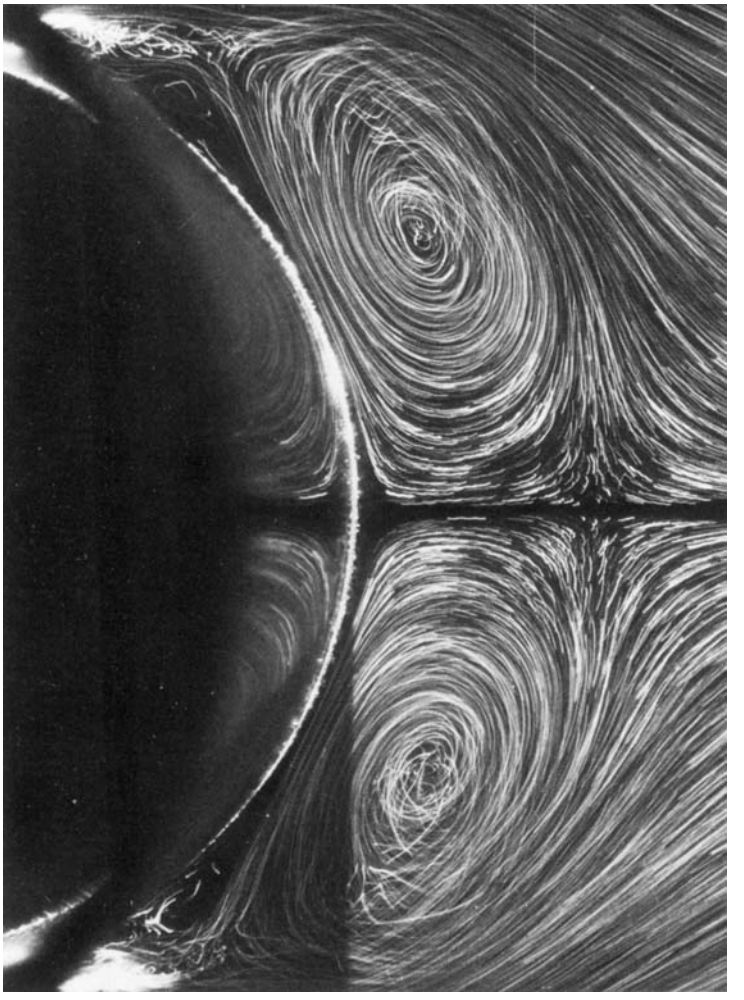

(*d*)

FIGURE 6. $Re = 9500$: (*a*) $t^* = 0{\cdot}75$, (*b*) $t^* = 1$, (*c*) $t^* = 1{\cdot}25$, (*d*) $t^* = 1{\cdot}5$.

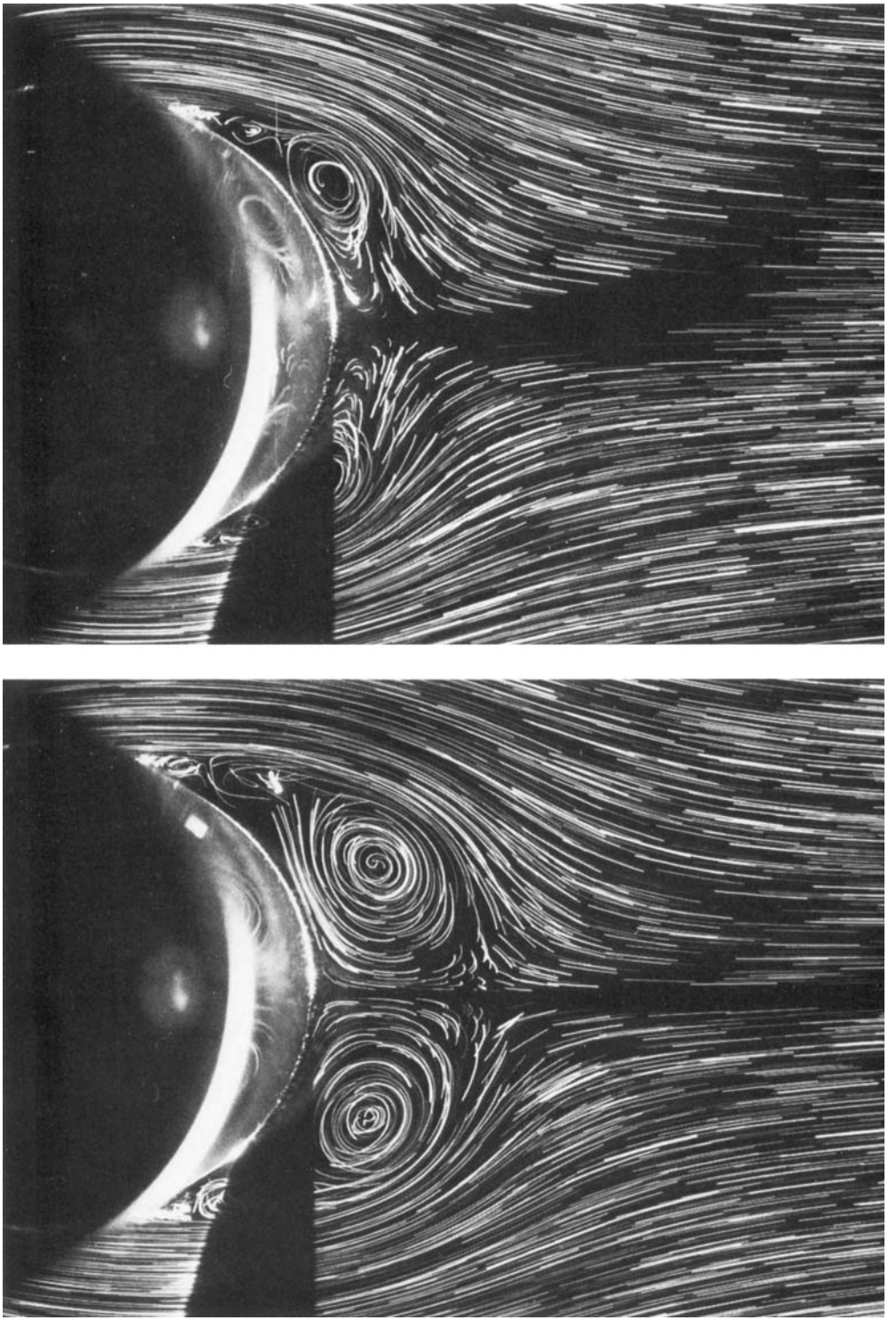

FIGURE 7 (*a*, *b*). For legend see plate 8.

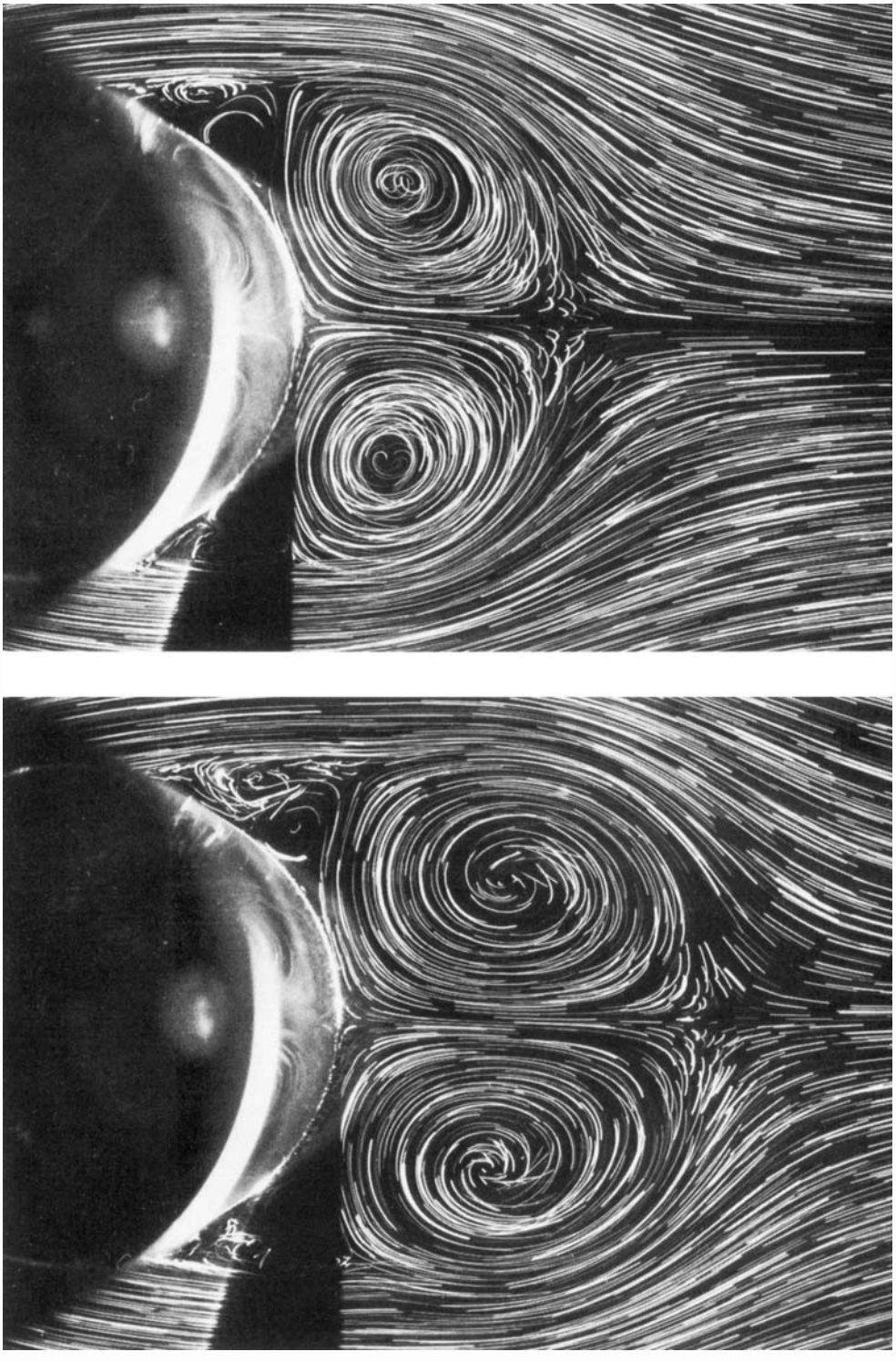

FIGURE 7. $Re = 5000$: (*a*) $t^* = 1$, (*b*) $t^* = 1{\cdot}5$, (*c*) $t^* = 2$, (*d*) $t^* = 2{\cdot}5$.